Journal of Materials Chemistry

Cite this: J. Mater. Chem., 2012, 22, 5349

www.rsc.org/materials

PAPER

Self-carbonized lamellar nano/micro hierarchical structure C/TiO_2 and its Li-ion intercalation performance†

Po-Chin Chen,[a] Min-Chiao Tsai,[a] Huang-Chin Chen,[e] I-Nan Lin,[e] Hwo-Shuenn Sheu,[d] Yu-Sheng Lin,[a] Jenq-Gong Duh,[a] Hsin-Tien Chiu[c] and Chi-Young Lee*[ab]

Received 23rd October 2011, Accepted 5th January 2012
DOI: 10.1039/c2jm15400e

In this study, two new layered titanates, fibrillar $TiO_2 \cdot (CH_3COOH)_{1.4}$ and chrysanthemum-like $TiO_2 \cdot (CH_3COOH)_{0.9}$ (named as FT and CT) with acetic acid and acetate intercalation have been synthesized by reacting titanium isopropoxide (TTIP) with acetic acid at different temperatures. Furthermore, nano/micro hierarchical structure TiO_2 with high TiO_2-B/anatse ratio was obtained by annealing the titanate (CT). For use as an anode for lithium ion batteries, uniform carbon coated titanium dioxide with high TiO_2-B content was obtained by "self-carbonizing" CT under argon atmosphere at 350 °C, and the compound was named SC-CT350. The capacity of the anode made from SC-CT350 can reach 144 mA h g^{-1} under a high charging/discharging rate (10 C) and showed excellent retention ability.

1. Introduction

Li-ion batteries are one of the promising energy storage devices to provide high efficiency, low cost and environmentally benign energy, and represents the state-of-the-art technology in rechargeable batteries because of their many advantages such as higher voltage, higher energy density, and longer cycle life compared with lead acid and Ni–Cd batteries. However, the efficiency of Li-ion batteries relies on the properties of the materials that are used to make the electrodes. Traditional materials for electrodes are often made by micrometre-sized materials and consequently limit the performance of Li-ion batteries due to the long diffusion length. There are two solutions to settle this kinetics problem: (1) decrease the diffusion distance, (2) enhance the diffusion coefficient of the materials. Recently, nanomaterials have played an important role in improving the performance of Li-ion batteries.[1–5] Scaling down particle size is one of the methods successfully employed in decreasing the diffusion length, which leads to the improvement of efficiency. For example, rutile TiO_2 has very inactive Li-ion diffusion along the (110) plane ($D_{(110)} \sim 10^{-15}$ cm^2s^{-1}). The mean diffusion time τ of micro-sized rutile and nano-sized rutile can be determined by the following equation:

$$\tau = L^2/2D \quad (1)$$

where L is diffusion length and D is the diffusion coefficient. For a 10 μm rutile particle, the mean diffusion time τ is *ca.* 3.8 years; however, this becomes 2 min for a 10 nm rutile particle.

The benefits from nanomaterials may not only cause shortening of the diffusion time, but also result in reducing the specific current density of the active materials, due to the larger surface area, and then enhance the rate performance. Therefore, the development of nanomaterials is thought to be a promising avenue towards vanquishing the current limits and achieving high performance Li-ion batteries. Despite having many merits, nanomaterials have some limitations too. The first is low thermodynamic stability due to their high surface area. This will cause the nanoparticles to tend to form agglomerates and will therefore result in an obstruction to mixing the active materials together with carbon black and binder to produce electrodes. Hence, non-uniform conductivity leads to polarization on the electrodes and induces fading in the capacity of the Li-ion battery. The second disadvantage of nanomaterials is high surface reactions. This will increase the hazard of undesirable reactions such as decomposition of electrolyte at the interface of the electrode and electrolyte and further induce considerable irreversible capacity, poor cycle life and safety issues.

In order to find a solution for the drawbacks of nanomaterials, one of the strategies employed is to develop nano/micro

[a]*Department of Materials Science and Engineering, National Tsing Hua University, 101, Sec. 2, Kuang-Fu Road, Hsinchu, Taiwan, R. O. C. E-mail: cylee@mx.nthu.edu.tw; Fax: + 886-3-5166687*
[b]*Center of Nanotechnology, Materials Science, and Microsystem, National Tsing Hua University, No. 101 Sec. 2 Kung Fu Rd, Hsinchu, Taiwan, R. O. C*
[c]*Department of Applied Chemistry, National Chiao Tung University, 1001, University Rd, Hsinchu, Taiwan, R. O. C. E-mail: htchiu@faculty.nctu.edu.tw*
[d]*Department of Physics, Tamkang University, 151, Yingzhuan Rd, Danshui Dist, New Taipei City, Taiwan, R. O. C*
[e]*Synchrotron Radiation Research Center, 101, Hsin-Ann Rd, Hsinchu, Taiwan, R. O. C*
† Electronic supplementary information (ESI) available. See DOI: 10.1039/c2jm15400e

hierarchical structures which are composed of nano-building blocks and micro-sized matrix. Electrode materials with these structures reveal good performance because they can grasp both the advantages of nano and micro materials. *i.e.* decrease the diffusion lengths by nano-building blocks; prevent agglomeration to promise good stability and easy fabrication.[6]

Recently, the ability of titanium oxide based materials to accommodate Li-ion makes them attractive and become one of the promising candidates for Li-ion batteries. Many investigations of titania and lithium titanate have been reported to develop synthetic methods and determine their electrochemical properties.[7–11] These include several kinds of various TiO_2 with different polymorphs, *i.e.* rutile,[12] anatase,[13] brookite,[14] TiO_2-B[15] and ramsdellite;[16] and two kinds of lithium titanates with different phases, *i.e.* spinel[17] and hexagonal structures.[18] Of these various kinds of titanium oxide based materials, TiO_2 with different polymorphs usually shows higher capacity than lithium titanate. This can be attributed to the theoretical capacity of TiO_2 being higher (334 mA h g^{-1}) than lithium titanate (*ca.* 170 mA h g^{-1}). Although TiO_2 can accommodate more Li-ions, lithium titanate can offer easier diffusion pathways for Li-ion due to its open structure and higher diffusion coefficient. Therefore, lithium titanate anodes usually show higher rate ability than TiO_2 anodes in previous studies.[19–21] However, amongst various TiO_2, TiO_2-B attracts more attention than other TiO_2 polymorphs because of its open structure. TiO_2-B is a metastable material which was first synthesized in 1980 by Marchand *et al.* from $K_2Ti_4O_9$ *via* K^+/H^+ ion exchange followed by calcination.[22] This synthetic strategy is also suitable for similar titanates such as sodium titanate and cesium titanate,[23,24] which can convert to hydrogen titanate by ion exchange and then further transform to TiO_2-B *via* thermal dehydratation. The open structure of TiO_2-B is constructed by layer structures in a lattice and stacking along *c*-axis with a large *d*-spacing. Hence, this results in the higher diffusion coefficient than other TiO_2 such as rutile and anatase, furthermore it also guarantees high rate efficiency.[25] For this reason, the synthetic methods and electrochemical properties of TiO_2-B have been widely studied.[26–28] Recently, we have also proposed a new method to synthesize TiO_2 nanosheets with TiO_2-B and anatase polymorphs *via* heating the HCOOH-intercalated titanate directly.[11] However, the anodes made by TiO_2-B also possessed poor conductivity like other TiO_2 polymorphs, which in turn once again leads fading of Li-ion battery capacity. Fortunately, doping or coating conductive materials on TiO_2 can improve this problem.[29–31] Recently, lots of attention has been paid to this area, due to the instability of the crystal structure, induced by doping. Thus, several kinds of conductive materials such as carbon and RuO_2 were used in the electrodes to enhance their poor conductivity. However, the challenge is how to make the conductive materials form an efficiently conductive network to transport the electrons and Li-ion in the active materials. Cao *et al.* have reported that carbon coated anatase TiO_2 can enhance the efficiency of Li-ion batteries due to the efficient mixed conducting 3D networks established when admixed with electronically conducting carbon black additive.[32] As the carbon coating processes are often operated at high temperature, TiO_2-B can be readily converted to anatase due to its thermal instability. Therefore, forming the uniform carbon network in the TiO_2 anode while keeping the quantity of TiO_2-B becomes more essential.

Here, we propose a simple strategy to synthesize an "acetate/AcOH-intercalated" titanate with nano/micro hierarchical structure. More interestingly, the large amount of acetic acids and acetate act not only as a component of the structure but also a carbon source. The uniform carbon networks inter/intra materials can be prepared by self-carbonizing of inserted acetic acid and the linked acetate without adding any carbon precursors. The coated carbon network in this work is different to others which have been reported so far.[29,30] The inter/intra carbon network provides an efficient electron/ion conducting ability and further shows enormous improvement as an anode for a Li-ion battery under high rate charge/discharge. Besides, a high quantity of layer TiO_2-B phase is transformed from titanate by direct calcination process. In this work, TiO_2-B phase together with a self-carbonized coating perform excellently as an anode material and showed the highest capacity (145 mA h g^{-1}) under high charging/discharging rate (10 C) amongst all of the TiO_2-B anodes which have been reported so far.

2. Experimental section

2.1 Preparation of TiO_2 material

2.1.1 Fibrillar TiO_2. In this work, all chemicals were purchased from Aldrich Company and directly used without further purification. The TiO_2 fibers were synthesized using titanium isopropoxide (TTIP, 97%, Aldrich) and acetic acid (98–100%, Aldrich) by a simple solvothermal method. The typical synthetic procedure is as follows. A solution of 0.3 mL TTIP (1 mmol) was injected into 10 mL acetic acid. Afterward, the solution was transferred into a Teflon-lined stainless steel autoclave (40 mL in volume) and then was sent into an air-flow electric oven. The resulting solution was heated at 125 °C for 48 h at the ramping rate of 5 °C per minute. After the completion of reaction, a white gel-like product was obtained. Subsequently, the product was sent into vacuum for 12 h. Hence, the white powder, fibrillar titanate, was obtained (hereafter referred as FT) and then was annealed at 500 °C for 8 h at the ramping rate of 3 °C per minute. The white powder after the annealing process is to referred as FT500 hereafter.

2.1.2 Chrysanthemum-like TiO_2. The synthesis of chrysanthemum-like TiO_2 was almost the same as FT except for the temperature. The solution was heated at 150 °C for 48 h and the ramping rate was 5 °C per minute. After the reaction completed, the precipitate was acquired by natural precipitation method. *i.e.* transferring the products to a centrifuge tube (20 mL in volume) and then allowing to stand for 24 h to separate into two layers. It can be observed clearly that the bottom layer is the white precipitate and the top layer is the solvent. Then, the solvent was removed by sending the products in a vacuum for 5 h. Hence, the white powder, chrysanthemum-like titanate, was obtained (hereafter referred to as CT). The products were heated under air at either 350 °C for 20 h or 500 °C for 8 h through a temperature ramping rate of 3 °C per minute and then cooled down to room temperature (hereafter the products are referred to as CT350 and

CT500 which were with different annealing temperature at 350 and 500 °C, respectively).

2.1.3 C/TiO_2 composites. The carbon coating on TiO_2 powder was carried out with two reaction conditions using different processes called the decomposition of ethanol and the self-carbonization method. For the first process, CT500 was prepared by chemical vapour deposition method using ethanol as the precursor and argon as the carrier gas. The flow rate of argon was 30 sccm and the powder was heated at 500 °C for 4 h and then was cooled down to room temperature. Finally, the black powder was collected (hereafter referred to as C-CT500). For the second process, as-prepared powder, CT, was annealed at 350 °C and 500 °C for about 20 h and 8 h under argon atmosphere respectively, which results in black powder (hereafter referred to as SC-CT350 and SC-CT500, respectively).

2.2 Characterization of TiO_2 material

SEM images were obtained using a JOEL-6500 field emission scanning electron microscope. TEM images were taken with a JOEL-2010 transmission electron microscope at an accelerating voltage of 200 kV. The structure of the powder was studied at the National Synchrotron Radiation Research Center (01C beam line). The incident X-ray energy in this work was 16 keV (λ = 0.774907 Å). Thermogravimetric analysis (TGA; Perkin Elmer) was done under air or N_2 flow of 30 mL min^{-1} from room temperature to 900 °C with a heating rate of 5 °C per minute. TGA-MASS was performed using the STA-409CD with Skimmer coupling from Netzsch, which is equipped with a quadrupole mass spectrometer QMA 400 from Balzers.

2.3 Electrochemical analysis

To appraise the efficiency of electrochemical anode in lithium-ion batteries, electrochemical cells were comprised of negative electrodes which were made by CT500, C-CT500, SC-CT500 and SC-CT350, respectively. Lithium metal was used as the counter and reference electrodes, and the electrolyte solution was 1.0 M $LiClO_4$ dissolved in a 1 : 1 mixture (by volume) of ethylene carbonate (EC) and diethyl carbonate (DEC). A Celgard 2400 membrane was used as the cell separator. The anode electrode which contained TiO_2/carbon composite (*i.e.* SC-CT350, SC-CT500 and C-CT500) was made by the mixture of 80 wt % active material, 10 wt % carbon black conducting agent (super P) and 10 wt % poly(vinylidene fluoride) (PVDF) as binder. The other anode electrode which contained only TiO_2 (*i.e.* CT500) as active material was made by the mixture of active material, super P and PVDF in a weight ratio of 70 : 20 : 10. After these materials had been mixed in an N-methyl-2-pyrrolidone (NMP) solution, the prepared slurry was coated on copper foil to a thickness of approximately 50 μm. After coating, the electrodes were dried at 110 °C for 2 h in the vacuum oven, to ensure that the solvent was evaporated, and subsequently roll-pressed. The 2032 coin-type cells were assembled in an argon-filled glove box and the charge/discharge tests were performed using an Arbin BT2000 at a constant current density with cutoff voltage of 3.0 V to 1.0 V.

3. Results and discussion

Fibrillar and chrysanthemum-like titanium oxides were synthesized by using titanium isopropoxide as a precursor *via* a simple solvothermal method under different reaction conditions. When titanium isopropoxide was added into acetic acid solution, the reaction occurred gently and the solution became turbid in a few minutes. This result was in contrast with our previous study in which the product precipitated immediately when injecting titanium isopropoxide into formic acid solution due to stronger acidity of formic acid.[11]

Fig. 1(a) is the image of the powder obtained at 125 °C for 48 h, which was denoted as fiber-like titanate (FT). The SEM image shows the fiber-like morphology, in which the length of each fiber varies from one to several micrometres and the thickness is about 25 nm. When the synthesis temperature was increased up to 150 °C, the precipitate (*chrysanthemum-like* titanate, CT) shows chrysanthemums 2–6 μm in diameter constructed of nano-sheets 3–15 nm thick (Fig. 1(c)). The energy-dispersive X-ray analysis (EDX) demonstrates that both FT and CT include only Ti, O and C (not shown). When the reaction time was shortened from 48 h to 18 h at 150 °C, both fiber and chrysanthemum-like products can be seen in the SEM image (Figure S1†). These results indicate that FT can be regarded as the precursor to form CT.

According to the X-ray diffraction pattern (XRD) shown in Fig. 2, both FT and CT are unknown crystalline structures with a peak in the low 2θ region, and the *d*-spacings of FT and CT are 13.9 and 11.3 Å, respectively. Usually, layerd titanates (*i.e.* $H_2Ti_3O_7$, $H_2Ti_4O_9 \cdot H_2O$, $K_2Ti_6O_{13}$ and $TiO_2 \cdot (HCOOH)_{0.9}$),[11,33,34] with organics, H_2O or cations inserted between the layers show a large *d*-spacing. However, such large *d*-spacings, 11.3 and 13.9 Å, have not been found in any present titanate and TiO_2. Therefore, it might be proposed that a large organic species such as AcOH or acetate exists in between the layers. Furthermore, the largest *d*-spacing of CT is 11.3 Å which is smaller than that in FT. In addition, the peaks related to the lattice spacing around 3.5 and 1.9 Å were found in both FT and CT. These observations are consistent with that by TEM (Figure S2†). As we know that anatase, TiO_2-B and most titanates built by zigzag sheets of TiO_6 octahedrons usually have *ca.* 3.5 and 1.9 Å lattice spacings, this indicates that CT and FT are constructed of zigzag sheets of TiO_6 octahedrons intercalated with organic fragments.[11]

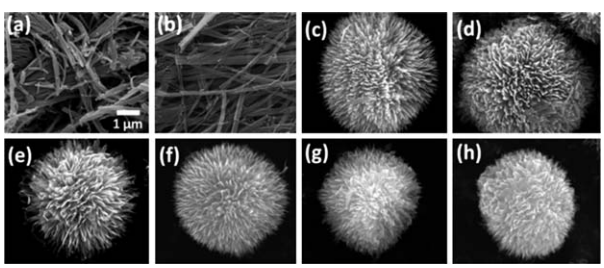

Fig. 1 SEM images of (a) FT, (b) FT500, (c) CT, (d) CT500, (e) CT350, (f) C-CT500, (g) SC-CT500 and (h) SC-CT350. The scale of all figures is the same.

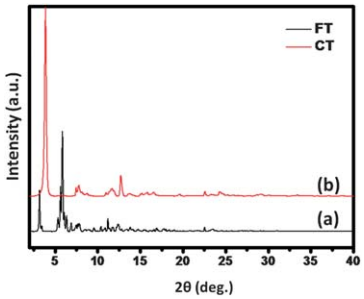

Fig. 2 X-ray diffraction (XRD) patterns of (a) FT and (b) CT.

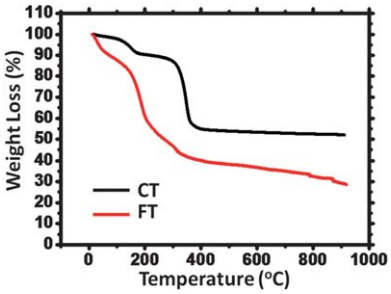

Fig. 4 Thermogravimetric analysis (TGA) of FT (red line) and CT (black line).

The organic fragment intercalation was further examined by FTIR study (Fig. 3). As we know that there are three bonding modes between titanium metal and acetate on titanium oxide surface, *i.e.* monodentate and bidentate (bridging and chelating), which could be recognized by the frequency difference between ν_{as} and ν_{s}, *i.e.* $\Delta\nu_{as\text{-}s}$. It has been reported that $\Delta\nu_{as\text{-}s}$ values are larger than 200 cm^{-1} in monodentate bonded acetate-Ti whereas the $\Delta\nu_{as\text{-}s}$ values of bidentate bonded acetate-Ti are often less than 160 cm^{-1}.[35] In this study, the peaks in the ranges of 1430–1470 cm^{-1} and 1520–1560 cm^{-1}were assigned to symmetric and asymmetric stretching vibrations of ν(COO) in acetate, respectively.[36] The $\Delta\nu_{as\text{-}s}$ values of FT and CT are both less than 160 cm^{-1}, and can be assigned to bidentate bonded acetate-Ti. In addition, the peaks at 1717 and 1721 cm^{-1} of FT and CT, respectively, which are in a lower carbonyl stretching frequency than those of acetic acid monomer (1780, 1795 cm^{-1}),[37] might be due to the dimer that is held together by hydrogen bonding between two monomers.[38] These results indicate that both acetic acid and acetate exist in FT and CT.

The quantities of the organic species in FT and CT were examined by TGA analysis (Fig. 4). The weight loss of FT and CT is 62% and 45.5%, respectively. The weight losses are much larger than that of sodium and hydrogen titanates which are usually in the range of 5–15%[39,40] but are similar to that of HCOOH-intercalated titanate. The weight loss of FT was continuous and the curve showed several different slopes as the temperature was incraesing, whereas the weight loss of CT occurred at two temperature regions, *i.e.* below 200 °C and over 350 °C.

TGA-MS was further employed to analyse the escaped species. Fig. 5 shows the 3-D diagram of FT and CT plotted against the ion current corresponding to *m*/*z* at different temperatures. The main peaks at *m*/*z* = 43 and 58 can be attributed to acetone, and the peaks at *m*/*z* = 43, 45 and 60 are contributed by acetic acid. The peaks at *m*/*z* = 60 can be observed around 160 °C in both FT and CT, and are assigned to acetic acid adsorbed on the samples surface. When the temperature was increased, the additional peak at *m*/*z* = 58 (assigned to acetone), accompanied with the peak of acetic acid (*m*/*z* = 60) was observed. According to the previous study,[41] many inorganic acetates can be decomposed at high temperature and produce acetone. Therefore, the significant acetone and AcOH peaks at higher temperature (250 °C for FT and 350 °C for CT) imply the intercalation of acetate and acetic acid, which was consistent with the FTIR observations. Otherwise, it's worth noting that the peaks related to the acetic acid dimer (*m*/*z* = 105 and 120) can also be observed in both FT and CT (Figure S3†), indicating that acetic acid exists in them in the form of dimers. Furthermore, the existence of acetic acid and acetate also provide a reasonable explanation for the larger *d*-spacing in FT (13.9 Å) and CT (11.3 Å) comparing to HCOOH-intercalated titanate (7.05 Å)[11] because the acetate and AcOH is larger than formate in geometry. At this stage, we know that the lattice structure of FT and CT may be constructed by TiO_6 octahedrons to form the layer structure with acetate and AcOH inserted in between the layers of the lattice, possible formulae for these two materials were derived as $TiO_2{\cdot}(CH_3COOH)_{1.4}$ and $TiO_2{\cdot}(CH_3COOH)_{0.9}$, according to 40% and 36% weight loss

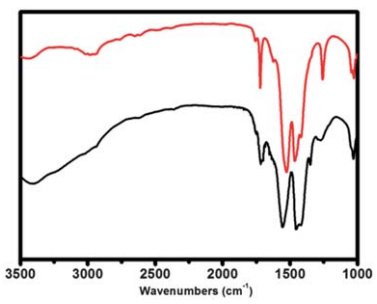

Fig. 3 Infrared (IR) spectra of FT (black line) and CT (red line). The peaks in the ranges of 1430–1460 cm^{-1} and 1520–1560 cm^{-1}, were assigned to symmetric and asymmetric stretching vibrations of ν(COO) in acetate, respectively. The peak at 1721 cm^{-1} was assigned to acetic acid.

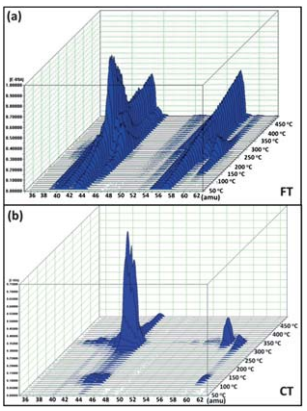

Fig. 5 TGA-MASS spectra of FT and CT.

measured by TGA after being heated over 150 °C for FT and CT, respectively. However, the exact lattice structures of both the new titanates are still unknown, the following studies are in progress presently.

It is known that hydrogen titanate is a metastable material and very easily converted to TiO_2-B or anatase by annealing at 350–500 °C, whereas, other metal titanates will not undergo any phase changes while heating at <400 °C, but can be transferred to anatase and rutile mixed phase over 500 °C.[22–24] As the FT and CT intercalated with organic species are also thermally unstable like hydrogen titanate, the phase transformations of FT and CT have been studied by XRD at various temperatures (Fig. 6). When FT was heated from room temperature to 500 °C, the crystalline structure initially collapsed and became amorphous at 350 °C, then, reconstructed to anatase phase at 500 °C. The SEM image of the powder after being annealed is shown in Fig. 1(b). Surprisingly, apart from a small amount of pores formed for FT, it maintained almost the same shape as prior to the annealing process. Even though FT would have sustained crystalline reconstruction, it appeared to have maintained its overall structural integrity which was unexpected. On the other hand, CT didn't undergo crystal reconstruction but directly transformed to metastable TiO_2-B and anatase phases coexisting at 350 °C. After annealing, the nanopores have formed on the nano sheets of the chrysanthemum TiO_2 (Figure S4†).

To consider the weight loss and layer spacing of FT and CT, a large amount of organic species intercalated in the FT matrix results in the large *d*-spacing and large weight loss, which lead to the structure collapsing and reconstructing as it was heated. Whereas, less organic species intercalated in CT resulted in smaller layer spacing and less weight loss, giving a direct phase transition upon heating.

According to the previous studies,[15,25–28,42,43] it is well known that TiO_2-B is a promising anode material for lithium ion batteries which can endure high rate charge/discharge due to its open structure. In this work CT having 3–15 nm thick nanosheets shows the ability to transform into TiO_2-B, which is suitable for acting as the anode in lithium ion batteries. After annealing the CT at 500 °C for 8 h (CT500), XRD pattern revealed that the treated sample consisted mainly of the anatase phase (Fig. 7). To obtain the optimal amount of crystalline TiO_2-B in the chrysanthemum-like TiO_2, CT was annealed at 350 °C for 20 h (CT350). According to the XRD patterns of CT350 and CT500, the peak intensity ratio of TiO_2-B/anatase in CT350 is higher than in CT500, this result clearly indicates that the quantity of TiO_2-B in CT350 is more than that of CT500, which was further confirmed by Raman spectra (Figure S5†).

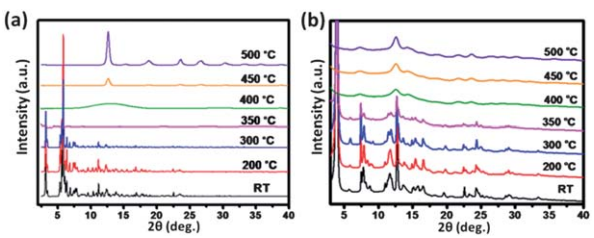

Fig. 6 *In situ* XRD with various temperatures of (a) FT and (b) CT.

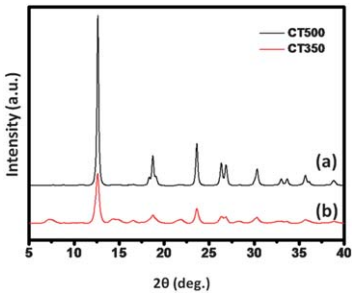

Fig. 7 X-ray diffraction (XRD) patterns of CT after annealing at (a) 500 °C for 8 h (CT500) and (b) 350 °C for 20 h (CT350).

The disadvantage of TiO_2 anodes of Li-ion batteries is the poor conductivity of TiO_2. Fortunately, the carbon coating on TiO_2 is one of the conventional methods to overcome this problem. According to the previous results (IR, TGA and TGA-MASS), we knew there were lots of organic species in CT. Furthermore, the differential scanning calorimetry (DSC) analysis of CT shows exothermic and endothermic peaks at *ca.* 350 °C under air and nitrogen atmospheres, respectively (Fig. 8). The appearance of an exothermic peak indicates the pyrolysis of the organic species in the material, whereas the appearance of an endothermic peak implies incomplete burning. Therefore, it is possible to use these organic species as the carbon source to form a carbon coating. The black powders, SC-CT350 and SC-CT500, were obtained as CT was heated at 350 °C for 20 h and 500 °C for 8 h under Ar atmosphere, respectively. Moreover, the additional nanopores formed by self-carbonizing on each nano sheets (Figure S1†), may facilitate the diffusion behaviour of Li-ions due to the higher interfacial area between the electrode and electrolyte.[10] On the other hand, a carbon layer was also coated on annealed CT (CT500) *via* thermal CVD using ethanol as precursor, the obtained powder was designated as C-CT500. The Raman spectra (Figure S6†) indicate that all the carbon coatings are amorphous. The thickness of the carbon layers is about 1–3 nm for SC-CT500 and SC-CT350, and 2–5 nm for C-CT500, as shown in HRTEM images (Fig. 9). In addition, the quantities of coated carbon with and without precursor determined by TGA are 8% and 4%, respectively (Figure S7†).

For the purpose of examining the capability of Li-ion intercalation, the Li-ion battery anodes were made by different TiO_2 polymorphs. Fig. 10 shows the electrochemical measurement results for the Li-ion battery anodes which were made by

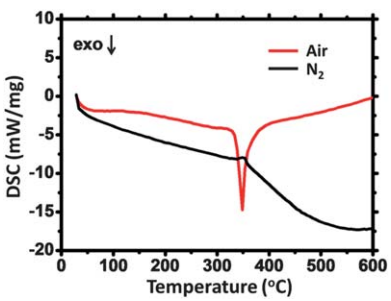

Fig. 8 Differential scanning calorimetry (DSC) analysis of CT under air (red line) and nitrogen atmosphere (black line).

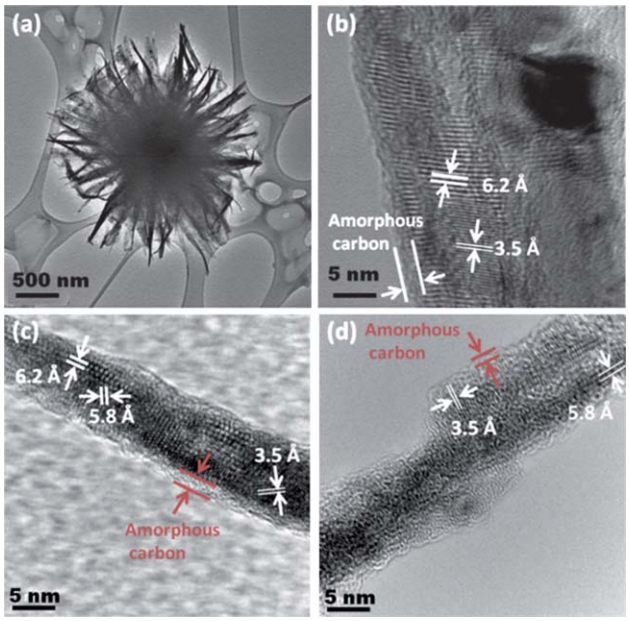

Fig. 9 TEM images of (a) C-CT500, and HETEM images of (b) C-CT500, (c) SC-CT500 and (d) SC-CT350. The 6.2 Å and 5.8 Å *d*-spacings belong to TiO_2-B; the 3.5 Å *d*-spacing belongs to anatase.

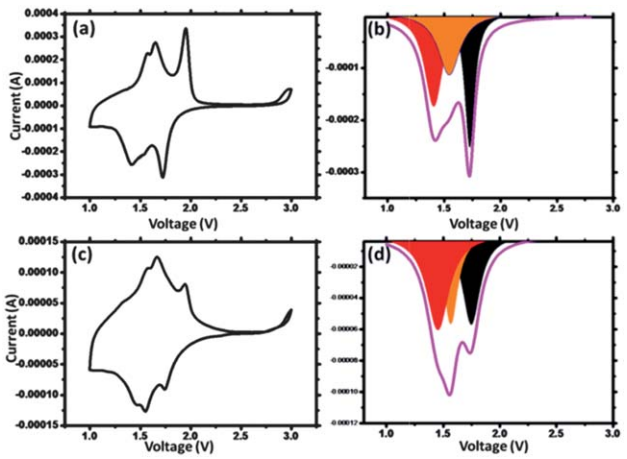

Fig. 10 CV curve and fitting peaks of galvanostatic discharging curve of the anode made by (a)(b) SC-CT500 and (c)(d) SC-CT350. The black areas refer to the anatase part, the orange and red areas refer to TiO_2-B.

SC-CT500 and SC-CT350. The CV profiles show three pairs of peaks, the two pairs of cathodic/anodic peaks at *ca.* 1.6–1.5 V were contributed by TiO_2-B,[44] whereas another pair of cathodic/anodic peaks at *ca.* 1.9 and 1.7 V were contributed by anatase.[45] Recently, the quantitative analysis of TiO_2-B studied by electrochemistry has been reported.[46] The TiO_2-B/anatase ratios estimated by electrochemistry peak areas are 53.2% and 65.2% for C-CT500 and SC-CT350, respectively.

Fig. 11 shows the performance of Li-ion batteries made by different TiO_2 polymorphs under different charge/discharge rates. The charge capacity of CT500 without carbon coating was 152 mA h g^{-1} in the first cycle then faded rapidly towards the 10th cycle. Finally, it was only 63 mA h g^{-1} in the 70th cycle at 1 C (334 mA g^{-1}) charge/discharge rate. However, the anode

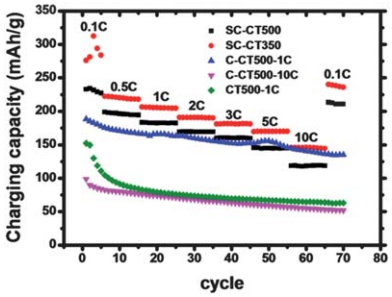

Fig. 11 Charging capacity of different anodes with various charging rates.

made by C-CT500, which contained only half the quantity of carbon black additive compared to the anode made by CT500, showed higher capacity than CT500 not only in the 1st cycle (183 mA h g^{-1}) but also in the 70th cycle (135 mA h g^{-1}) at 1 C charging/discharging rate. This result indicates that even CT500 has a porous morphology like C-CT500, but only carbon coated TiO_2 can improve the poor conductivity of TiO_2, decrease the inner resistance of the anode and then enhance the performance, as in the previous reports.[29,30] Nevertheless, as C-CT500 under 10 C charging/discharging rate can reach only 99 mA h g^{-1} at the first cycle and remain at 52 mA h g^{-1} at the 70th cycle, both SC-CT500 and SC-CT350 showed good performance under various charging/discharging rates (0.1 C to 10 C). SC-CT500 can keep the capacity at 183 and 119 mA h g^{-1} without deterioration under 1 C and 10 C charging rate, respectively. Furthermore, SC-CT350 exhibited greater cycleability (206 and 145 mA h g^{-1} at 1 C and 10 C, respectively) than SC-CT500. Moreover, both SC-CT350 and SC-CT500 showed good reversibility (Figure S8†). The SC-CT350 and SC-CT500 powders obtained by the self-carbonized method are superior to carbon coated C-CT500 obtained by the CVD process. The improvement in the performance may be due to the architectures of the carbon networks, resulting from the different carbon coating procedures, as shown in Scheme 1. The coating procedure for C-CT500 contained two steps. The first step was

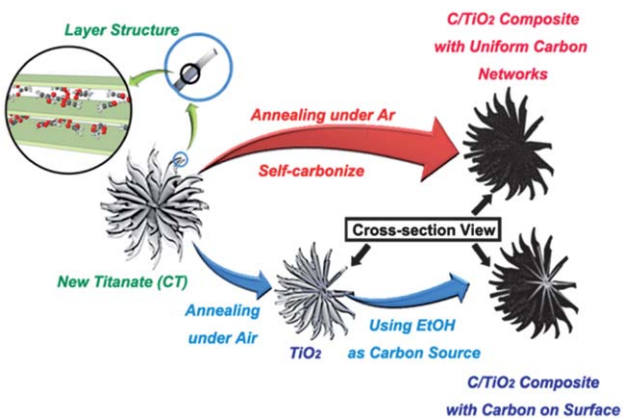

Scheme 1 Partial enlarged drawing of CT (shows layer structure with organic species inserted) and two different procedures to form C/TiO_2 composites with and without precursors (shown by the blue and the red arrow, respectively).

annealing of CT at 500 °C to TiO_2. In the second step, carbon was coated on the TiO_2 by thermal decomposition of added ethanol, which results in the carbon only being coated on the surface of each particle on the TiO_2 and so the conductivity inside the surface of TiO_2 particles remains still poor. Therefore, the anode of C-CT500 exhibited the polarization gradually while increasing the cycle at high rate, which leads fading in capacity (Figure S9†). However, the single-step "self-carbonizing" overcame this drawback due to the formation of the uniform carbon networks as shown in Scheme 1. The discharge curves with different cycles almost overlapped together and were hard to distinguished from each other, indicating that the capacity retention ability was not hindered by the polarization of the anode while increasing the cycle. On the other hand, considering the greater performance of SC-CT350 than SC-CT500, the quantity of TiO_2-B played an important role to provide kinetically high diffusion coefficient and high rate ability.

4. Conclusions

In conclusion, fibrillar and chrysanthemum-like titanates with acetate and acetic acid intercalation (FT and CT, respectively) have been synthesized. The molecule acetic acid was in between the layers of the lattice in dimer form, and the acetate bonded to Ti atoms as bidentate mode. Moreover, CT can further transform to TiO_2 and C/TiO_2 with anatase/TiO_2-B polymorphs under different thermal conditions. The chrysanthemum-like C/TiO_2 composites with nano/micro hierarchical porous structure, SC-CT500 and SC-CT350, with uniform carbon coating and a high quantity of TiO_2-B were obtained in one step through annealing the CT under an Ar atmosphere. The high charging/discharging rate (10 C) performance of Li-ion batteries which were made by SC-CT500 (119 mAh/g) and SC-CT350 (145 mAh/g) benefited from the short diffusion length of nano-sheets with nanopores, high diffusion coefficient of TiO_2-B and the uniform carbon coating on the particles. The good cycleability and the rate efficiency are both proportional to the quantity of TiO_2-B in the materials.

Acknowledgements

The authors would like to thank the National Science Council of the Republic of China, Taiwan, for financially supporting this research under contract no. NSC-97-2113-M-009-015-MY3 and NSC-99-2113-M-007-011.

References

1 P. Balaya, *Energy Environ. Sci.*, 2008, **1**, 645–654.
2 W. J. H. Borghols, M. Wagemaker, U. Lafont, E. M. Kelder and F. M. Mulder, *Chem. Mater.*, 2008, **20**, 2949–2955.
3 W. J. H. Borghols, M. Wagemaker, U. Lafont, E. M. Kelder and F. M. Mulder, *J. Am. Chem. Soc.*, 2009, **131**, 17786–17792.
4 C. H. Jiang, M. D. Wei, Z. M. Qi, T. Kudo, I. Honma and H. S. Zhou, *J. Power Sources*, 2007, **166**, 239–243.
5 Y. S. Lin, J. G. Duh and M. H. Hung, *J. Phys. Chem. C*, 2010, **114**, 13136–13141.
6 Y. G. Guo, J. S. Hu and L. J. Wan, *Adv. Mater.*, 2008, **20**, 4384–4384.
7 W. J. H. Borghols, D. Lutzenkirchen-Hecht, U. Haake, W. Chan, U. Lafont, E. M. Kelder, E. R. H. van Eck, A. P. M. Kentgens, F. M. Mulder and M. Wagemaker, *J. Electrochem. Soc.*, 2010, **157**, A582–A588.
8 M. Bousa, B. Laskova, M. Zukalova, J. Prochazka, A. Chou and L. Kavan, *J. Electrochem. Soc.*, 2010, **157**, A1108–A1112.
9 S. Kerisit, K. M. Rosso, Z. G. Yang and J. Liu, *J. Phys. Chem. C*, 2010, **114**, 19096–19107.
10 K. Saravanan, K. Ananthanarayanan and P. Balaya, *Energy Environ. Sci.*, 2010, **3**, 939–948.
11 M. C. Tsai, J. C. Chang, H. S. Sheu, H. T. Chiu and C. Y. Lee, *Chem. Mater.*, 2009, **21**, 499–505.
12 Y. S. Hu, L. Kienle, Y. G. Guo and J. Maier, *Adv. Mater.*, 2006, **18**, 1421.
13 M. S. Wu, M. J. Wang, J. J. Jow, W. D. Yang, C. Y. Hsieh and H. M. Tsai, *J. Power Sources*, 2008, **185**, 1420–1424.
14 M. A. Reddy, M. S. Kishore, V. Pralong, U. V. Varadaraju and B. Raveau, *Electrochem. Solid-State Lett.*, 2007, **10**, A29–A31.
15 L. Kavan, M. Kalbac, M. Zukalova, I. Exnar, V. Lorenzen, R. Nesper and M. Graetzel, *Chem. Mater.*, 2004, **16**, 477–485.
16 A. Kuhn, R. Amandi and F. Garcia-Alvarado, *J. Power Sources*, 2001, **92**, 221–227.
17 M. Wagemaker, D. R. Simon, E. M. Kelder, J. Schoonman, C. Ringpfeil, U. Haake, D. Lutzenkirchen-Hecht, R. Frahm and F. M. Mulder, *Adv. Mater.*, 2006, **18**, 3169.
18 T. A. Hewston and B. L. Chamberland, *J. Phys. Chem. Solids*, 1987, **48**, 97–108.
19 A. S. Prakash, P. Manikandan, K. Ramesha, M. Sathiya, J. M. Tarascon and A. K. Shukla, *Chem. Mater.*, 2010, **22**, 2857–2863.
20 P. P. Prosini, R. Mancini, L. Petrucci, V. Contini and P. Villano, *Solid State Ionics*, 2001, **144**, 185–192.
21 A. D. Robertson, L. Trevino, H. Tukamoto and J. T. S. Irvine, *J. Power Sources*, 1999, **81**, 352–357.
22 R. Marchand, L. Brohan and M. Tournoux, *Mater. Res. Bull.*, 1980, **15**, 1129–1133.
23 T. P. Feist and P. K. Davies, *J. Solid State Chem.*, 1992, **101**, 275–295.
24 T. P. Feist, S. J. Mocarski, P. K. Davies, A. J. Jacobson and J. T. Lewandowski, *Solid State Ionics*, 1988, **28**, 1338–1343.
25 M. Inaba, Y. Oba, F. Niina, Y. Murota, Y. Ogino, A. Tasaka and K. Hirota, *J. Power Sources*, 2009, **189**, 580–584.
26 A. R. Armstrong, G. Armstrong, J. Canales and P. G. Bruce, *Angew. Chem., Int. Ed.*, 2004, **43**, 2286–2288.
27 C. Arrouvel, S. C. Parker and M. S. Islam, *Chem. Mater.*, 2009, **21**, 4778–4783.
28 M. Wilkening, J. Heine, C. Lyness, A. R. Armstrong and P. G. Bruce, *Phys. Rev. B*, 2009, 80.
29 S. K. Das, S. Darmakolla and A. J. Bhattacharyya, *J. Mater. Chem.*, 2010, **20**, 1600–1606.
30 Y. Ishii, Y. Kanamori, T. Kawashita, I. Mukhopadhyay and S. Kawasaki, *J. Phys. Chem. Solids*, 2010, **71**, 511–514.
31 B. M. S. Yude Wang and Igor Djerdj, *Chem. Mater.*, 2010, **22**, 6624–6631.
32 F. F. Cao, X. L. Wu, S. Xin, Y. G. Guo and L. J. Wan, *J. Phys. Chem. C*, 2010, **114**, 10308–10313.
33 G. H. Du, Q. Chen, P. D. Han, Y. Yu and L. M. Peng, *Phys. Rev. B*, 2003, 67.
34 A. Nakahira, W. Kato, M. Tamai, T. Isshiki, K. Nishio and H. Aritani, *J. Mater. Sci.*, 2004, **39**, 4239–4245.
35 G. B. Deacon and R. J. Phillips, *Coord. Chem. Rev.*, 1980, **33**, 227–250.
36 S. Doeuff, Y. Dromzee, F. Taulelle and C. Sanchez, *Inorg. Chem.*, 1989, **28**, 4439–4445.
37 R. C. Herman and R. Hofstadter, *J. Chem. Phys.*, 1938, **6**, 534–540.
38 L. F. Liao, C. F. Lien and J. L. Lin, *Phys. Chem. Chem. Phys.*, 2001, **3**, 3831–3837.
39 E. Morgado, M. A. S. de Abreu, G. T. Moure, B. A. Marinkovic, P. M. Jardim and A. S. Araujo, *Chem. Mater.*, 2007, **19**, 665–676.
40 A. L. Sauvet, S. Baliteau, C. Lopez and P. Fabry, *J. Solid State Chem.*, 2004, **177**, 4508–4515.
41 M. D. Judd, B. A. Plunkett and M. I. Pope, *J. Therm. Anal.*, 1974, **6**, 555–563.
42 G. Armstrong, A. R. Armstrong, P. G. Bruce, P. Reale and B. Scrosati, *Adv. Mater.*, 2006, **18**, 2597.
43 M. Wilkening, C. Lyness, A. R. Armstrong and P. G. Bruce, *J. Phys. Chem. C*, 2009, **113**, 4741–4744.
44 M. Zukalova, M. Kalbac, L. Kavan, I. Exnar and M. Graetzel, *Chem. Mater.*, 2005, **17**, 1248–1255.
45 L. Kavan, J. Rathousky, M. Gratzel, V. Shklover and A. Zukal, *J. Phys. Chem. B*, 2000, **104**, 12012–12020.
46 T. Beuvier, M. Richard-Plouet and L. Brohan, *J. Phys. Chem. C*, 2009, **113**, 13703–13706.